Study of the atmospheric pressure loading signal in very long baseline interferometry observations

Leonid Petrov and Jean-Paul Boy[1]

NVI, Inc./NASA Goddard Space Flight Center, Greenbelt, Maryland, USA

[1]   Redistribution of air masses due to atmospheric circulation causes loading deformation of the Earth's crust, which can be as large as 20 mm for the vertical component and 3 mm for horizontal components. Rigorous computation of site displacements caused by pressure loading requires knowledge of the surface pressure field over the entire Earth surface. A procedure for computing three-dimensional displacements of geodetic sites of interest using a 6 hourly pressure field from the National Centers for Environmental Prediction numerical weather models and the *Ponte and Ray* [2002] model of atmospheric tides is presented. We investigated possible error sources and found that the errors of our pressure loading time series are below the 15% level. We validated our model by estimating the admittance factors of the pressure loading time series using a data set of 3.5 million very long baseline interferometry observations from 1980 to 2002. The admittance factors averaged over all sites are 0.95 ± 0.02 for the vertical displacement and 1.00 ± 0.07 for the horizontal displacements. For the first time, horizontal displacements caused by atmospheric pressure loading have been detected. The closeness of these admittance factors to unity allows us to conclude that on average, our model quantitatively agrees with the observations within the error budget of the model. At the same time we found that the model is not accurate for several stations that are near a coast or in mountain regions. We conclude that our model is suitable for routine data reduction of space geodesy observations.   *INDEX TERMS:* 1223 Geodesy and Gravity: Ocean/Earth/atmosphere interactions (3339); 1247 Geodesy and Gravity: Terrestrial reference systems; 1294 Geodesy and Gravity: Instruments and techniques; *KEYWORDS:* atmospheric pressure loading, VLBI

1.   Introduction

[2]   At the level of precision of modern space geodetic techniques the Earth's crust is not static, but deformable. The Earth's crust deformation can be caused by processes inside the Earth, by gravitational forces of external celestial bodies, by changes of the centrifugal potential, and by various mass loads. Analysis of geodetic observations made from the deformable surface of our planet requires applying a model of these deformations. The precision of this model should be comparable with the precision of the measurements, otherwise unaccounted site position variations due to crust deformation become a factor which limits the accuracy of measurements, and the potential of geodetic techniques cannot fully be exploited.

[3]   In this paper we focus on the Earth's crust deformation caused by the load of the atmosphere. As was found by E. Torricelli in 1644 [*Magie*, 1963], the atmospheric pressure is not constant, but has variations at the level of 20–50 mbar. *Darwin* [1882] was the first who realized that this can cause deformation at the level of several centimeters, and he proposed a simple model for its computation. However, before the advent of space geodesy, quasi-random site displacements at the level of centimeters were not directly measurable and, therefore, there was no necessity to take them into account.

[4]   Rapid development of space geodetic techniques in the 1980s made it feasible to try to detect atmospheric pressure loading signal from the measurements of site positions. *Trubytsyn and Makalkin* [1976] and later *Rabbel and Zschau* [1985], *Rabbel and Schuh* [1986] and *vanDam and Wahr* [1987] made quantitative assessments of the impact of passing cyclones and anticyclones on measurements of site positions assuming that the pressure distribution in cyclones or anticyclones can be described by a simple mathematical model. *Manabe et al.* [1991] tried to find a correlation between predicted atmospheric pressure loading and the time series of site position determined from very long baseline interferometry (VLBI) observations during 1984–1989 at several stations, but had to acknowledge that the observationally determined vertical displacements are [*Manabe et al.*, 1991, p. 122] "not explainable as

_____
[1]Now at Ecole et Observatoire des Sciences de la Terre, Université Strasbourg, Strasbourg, France.

being caused by the atmospheric loading, since the dispersion of the observed vertical displacements is too large." Three years later *vanDam and Herring* [1994] and independently *MacMillan and Gipson* [1994] succeeded in detecting atmospheric pressure loading signal using more sophisticated approaches. *MacMillan and Gipson* [1994] estimated coefficients of linear regression between vertical site displacements and local pressure using VLBI data. They found that these coefficients for the majority of sites are in reasonable agreement with the coefficients derived by *Manabe et al.* [1991], and that applying an empirical model based on the regression between vertical site position and local pressure improves baseline length repeatability. *vanDam and Herring* [1994] (hereinafter referred as VDH) used another approach. They analyzed the reduction of variance of the estimates of baseline lengths derived from analysis of the same VLBI data set. They found that the reduction of variance is consistent with the hypothesis that only approximately 60% of the computed pressure loading contribution is present in the VLBI length determination. Applying the same technique to global positioning system (GPS) data allowed *vanDam et al.* [1994] to conclude that 57% of the pressure loading signal is present in the baseline length residuals.

[5] Although the presence of atmospheric pressure loading signal was confirmed in observations, modeling this signal did not come into practice for routine data reduction. First, a rigorous computation of displacements caused by mass loading requires handling a gigantic volume of information and enormous processor power. Second, there was no certainty whether the model is correct. Results of VDH and *vanDam et al.* [1994] mean that observations did not confirm quantitatively the atmosphere pressure loading model. Without solving this discrepancy, applying the atmosphere pressure loading model for processing routine observations is not warranted.

[6] There are several factors that motivated us to revisit this topic. First, the National Centers for Environmental Prediction (NCEP) Reanalysis project [*Kalnay et al.*, 1996] now provides a continuous, uniform data set of surface pressure on a 2.5° × 2.5° grid with a 6 hour resolution for more than 40 years which was not available a decade ago. Second, rapid development of high-speed networks and processor power makes it possible to retrieve and process voluminous meteorological data assimilation models in almost real time. Third, the accuracy of geodetic observations has increased considerably during the last ten years, which has improved our ability to detect subtle Earth's crust motions.

[7] The objective of our study was to develop a procedure of computing displacements caused by atmospheric pressure loading which is suitable for routine analysis of geodetic observations, and to compare these time series of pressure loading with a data set of all VLBI observations from 1980 to 2002. The purpose of this comparison is to get a quantitative measure of the agreement between the model and observations, and infer whether the model is correct or wrong. In order to do it, we thoroughly examine the error budget and on the basis of these estimates compute the expectation of the deviation of the observations from the model. Our goal is to determine whether the observations deviate from the expectation or not. If the agreement test

deviates from the expectation at a statistically significant level, this means that either there is an error in computations or there is a fundamental flaw in our understanding of the physics of the phenomena under consideration. Then the model must be rejected at this point. If the outcome of the statistical test is within the predicted range based on known deficiencies of the model, this means that the procedure for computation of the atmosphere pressure loading can be accepted for routine reduction of observations.

[8] In the second section of the paper we describe our method of computing site displacements caused by pressure loading and assess the error budget of our calculations. We reanalyzed a data set of 3.5 million VLBI observations and performed several statistical tests of agreement between the model of pressure loading and the observations. The method of data analysis is described in section 3. The results of the VLBI data analysis are discussed in section 4. Concluding remarks are given in section 5. An efficient procedure for computing a time series of pressure loading is outlined in Appendix A.

2. Computation of Displacements Using Meteorological Models

[9] According to *Farrell* [1972] the vertical displacement at a station with coordinates $\vec{r}$ induced by surface pressure variations $\Delta P(\vec{r}', t)$ is

$$u_r(\vec{r}, t) = \iint \Delta P(\vec{r}', t)\, G_R(\psi) \cos \varphi'\, d\lambda'\, d\varphi'. \qquad (1)$$

The vertical Green's function is

$$G_R(\psi) = \frac{fa}{g_0^2} \sum_{n=0}^{+\infty} h_n' P_n(\cos \psi), \qquad (2)$$

where f, a and g_0 are the universal constant of gravitation, the mean Earth's radius and the mean surface gravity as defined in PREM [*Dziewonski and Anderson*, 1981], φ' is the geocentric latitude, and λ' is the longitude. ψ is the angular distance between the station with coordinates $\vec{r}$ and the pressure source with coordinates $\vec{r}'$. P_n is the Legendre polynomial of degree n.

[10] The horizontal displacement is computed this way:

$$\vec{u}_h(\vec{r}, t) = \iint \vec{q}(\vec{r}, \vec{r}')\, \Delta P(\vec{r}', t) G_H(\psi) \cos \varphi'\, d\lambda'\, d\varphi', \qquad (3)$$

where $\vec{q}(\vec{r}, \vec{r}')$ is the unit vector originating from the station, tangential to the Earth's surface, which lies in the plane determined by the radius vectors to the station and to the pressure source. The tangential Green's function is [*Farrell*, 1972]

$$G_H(\psi) = -\frac{fa}{g_0^2} \sum_{n=1}^{+\infty} l_n' \frac{\partial P_n(\cos \psi)}{\partial \psi}. \qquad (4)$$

Numerical evaluation of the Green's function requires the computation of load Love numbers h_n' and l_n' up to a high spherical harmonic degree (n = 9000 in this study) for a spherically symmetric, nonrotating, elastic and isotropic

(SNREI) Earth model. The method of numerical computation of Green's functions is presented by *Farrell* [1972].

[11] We model the oceanic response to atmospheric pressure forcing as an inverted barometer (IB):

$$\Delta P_a + \Delta P_w - \Delta \bar{P}_o = 0, \tag{5}$$

where ΔP_a is the variation of local atmosphere pressure, ΔP_w is the local variation of the ocean bottom pressure due to induced sea level change, and $\Delta \bar{P}_o$ is the mean atmosphere pressure over the world's oceans:

$$\Delta \bar{P}_o = \frac{\iint\limits_{ocean} \Delta P(\vec{r}', t) \cos \varphi' d\lambda' d\varphi'}{\iint\limits_{ocean} \cos \varphi' d\lambda' d\varphi'}, \tag{6}$$

which is applied uniformly at the sea floor [*vanDam and Wahr*, 1987]. This term is introduced in equation (5) in order to enforce conservation of ocean mass. Thus the total ocean bottom pressure, $\Delta P_a + \Delta P_w$, is described by equation (6). It has been shown in numerous studies [see, e.g., *Tierney et al.*, 2000] that this model adequately describes the sea height variations for periods longer than 5–20 days. However, the ocean response significantly deviates from the IB hypothesis for shorter periods [*Wunsch and Stammer*, 1997].

[12] Since $\Delta \bar{P}_o$ is zero over the land and depends only on time over the world's oceans, it is convenient to split integrals (1) and (3) into a sum of integrals over the ocean and over the continental surface. In our computation we use the land-sea mask from the FES99 [*Lefèvre et al.*, 2002] ocean tidal model with a 0.25° spatial resolution. A practical algorithm for the computation of site displacements caused by atmospheric pressure loading is presented in Appendix A.

[13] Since the NCEP Reanalysis numerical weather models have a time resolution of 6 hours, the semidiurnal (S_2) atmospheric tide induced by solar heating cannot be modeled correctly, because its frequency corresponds exactly to the Nyquist frequency. The diurnal (S_1) atmospheric tide is somewhat distorted as well, because of the presence of the ter-diurnal signal, which is folded into the diurnal frequency due to sampling. This problem was investigated by *van den Dool et al.* [1997] in detail, who proposed a temporal interpolation procedure which to some extent allows one to overcome the problem. On the basis of this approach *Ponte and Ray* [2002] recently developed a gridded global model of the S_1 and S_2 atmospheric tides with a spatial resolution of 1.125° × 1.125°. For reasons discussed by these authors, we believe their model better represents the atmospheric tides than the diurnal and semidiurnal signal which is present in the NCEP Reanalysis model. Using these maps we have computed amplitudes and phases of the loading caused by diurnal and semidiurnal atmospheric tides for VLBI and satellite laser ranging (SLR) sites.

[14] For each grid point we have estimated four parameters using least squares (LSQ): mean pressure, sine and cosine amplitude of the S_1 signal, and cosine amplitude of the S_2 signal in the surface pressure field over the time period from 1980 to 2002. This four-parameter model is subtracted at each point of the grid from the NCEP Reanalysis pressure field before evaluation of the convolution integral. Thus our time series has zero mean and no signal at S_1 and S_2 frequencies. The total loading is the sum of the time series and the harmonic model of the S_1 and S_2 loading caused by atmospheric tides.

2.1. Characteristics of the Atmospheric Pressure Loading Displacements

[15] In Figures 1 and 2 we show examples of time series of the modeled displacements for the period 2000–2003 and their power spectrum at the Wettzell and Hartrao stations respectively. These stations are representative of midlatitude and equatorial inland stations.

[16] All station displacements show significant narrow-band diurnal and semidiurnal signals. The displacements for low-latitude stations are characterized by a strong wide-band annual and semiannual signals and relatively weak signal for periods below 10 days, except strong peaks at the S_1 and S_2 frequencies. Midlatitude stations show just the opposite behavior. For the midlatitude regions circulation of low-pressure and high-pressure structures with periods of 5–10 days is typical. These periods are also at the edge of the validity of the IB model for describing the oceanic response to atmospheric pressure forcing.

[17] The rms of vertical and horizontal displacements is presented in columns 4 and 5 of Table 1. Figure 3 shows an example of the temporal autocorrelation function for the vertical displacement for the midlatitude station Algopark. The autocorrelation rapidly drops to the level less than 0.2 for time intervals longer than 2 days. The smoothed spatial autocorrelation of the vertical displacement induced by atmospheric pressure loading is presented in Figure 4. We see that the correlation for baselines shorter than 1000 km is very high, typically greater than 0.9, and only for baselines longer than 3000 km does it drop below the level of 0.2.

2.2. Error Budget

[18] There are four major sources of errors in the computation of site displacements caused by atmospheric pressure loading: (1) errors in the Green's functions; (2) errors in the land-sea mask; (3) errors in the pressure field; and (4) mismodeling the ocean response to atmospheric pressure forcing.

[19] The Green's functions are computed for a SNREI Earth model adopting PREM elastic parameters. Thus we neglect the effects induced by Earth's anelasticity and ellipticity. The differences between our Green's functions and Green's functions for an anelastic Earth model [see, e.g., *Pagiatakis*, 1990; *Okubo and Tsuji*, 2001] are typically below 1–2%. The effect of the Earth's ellipticity is of the order of magnitude of the Earth's flattening, i.e., 0.3%.

[20] Since the 2.5° spatial resolution of the NCEP Reanalysis surface pressure field is not sufficient to correctly represent the coastline, we chose a land-sea mask with a 0.25° resolution from the FES99 [*Lefèvre et al.*, 2002] ocean tidal model. The land-sea mask and the station distribution are shown in Figure 5. We assume that enclosed and small semienclosed seas (such as Baltic, Black, Red, Caspian Seas and Persian Gulf) respond to atmospheric pressure forcing as a "noninverted barometer"; that is,
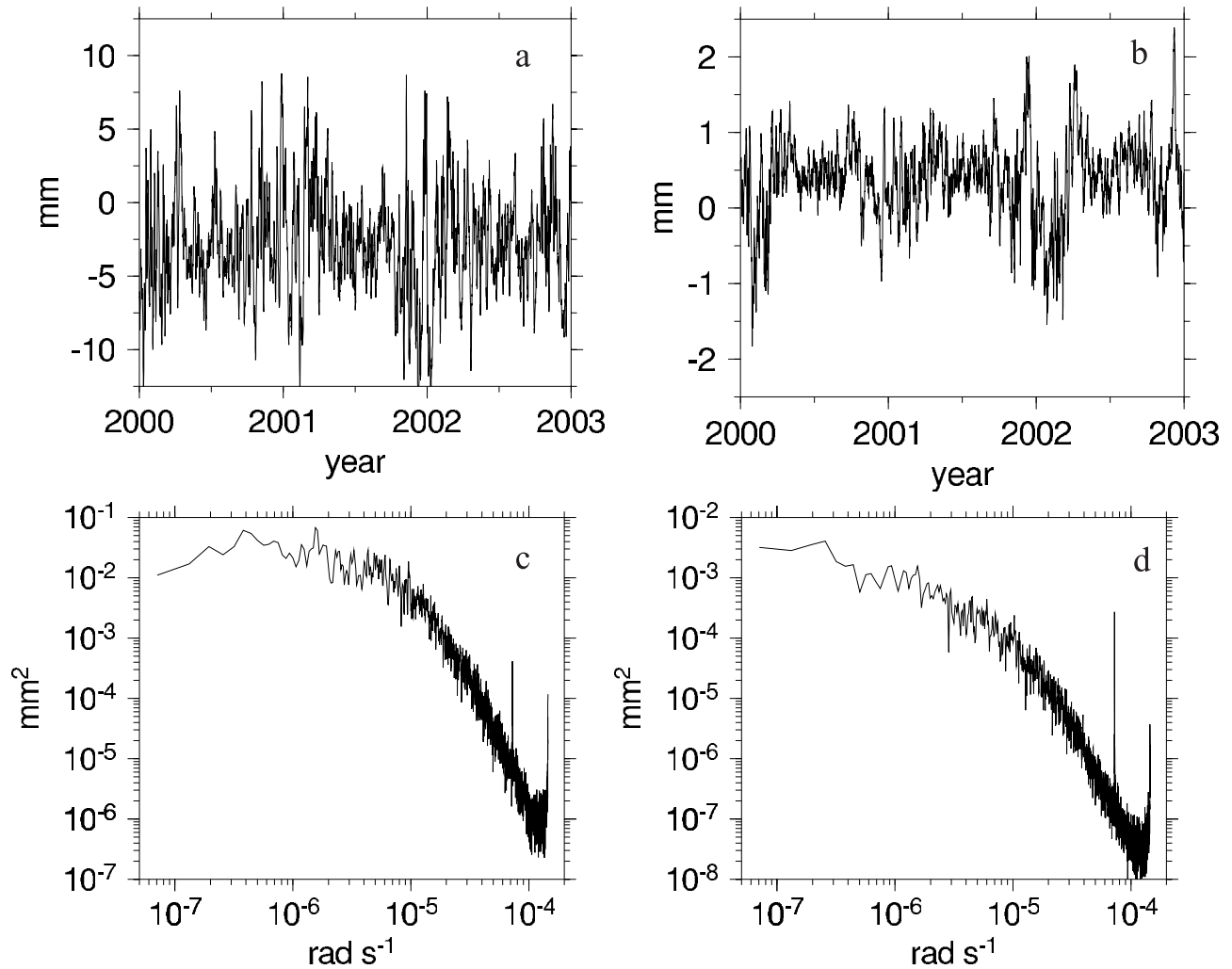
Figure 1. (a) Vertical and (b) north displacements induced by atmospheric pressure loading at the station Wettzell. Power spectrum of the (c) vertical and (d) north displacements.

atmospheric pressure variations are fully transmitted to the sea floor. In order to evaluate the effect of the errors in the land-sea mask, we computed the time series of atmospheric pressure loading with both the 0.25° and 0.50° land-sea masks. The differences between these two estimates are typically about 5%. It is worth mentioning that the difference between the loading estimates with the 2.5° and 0.25° land-sea masks can reach 10% for the vertical component and 30% for the horizontal components, even for a station like Wettzell (Germany) which is 500 km from the coast.

[21] Another source of error in our computations are errors in the surface pressure field from the NCEP Reanalysis. One way to compute this is to compare directly the difference between the model and surface pressure observations. *Velicogna et al.* [2001] presented estimates of the rms differences for two different regions (Arabic Peninsula and United States). On the basis of their estimates we conclude that the errors of the NCEP surface pressure field on these selected areas are at the level of 5%.

[22] Another measure of possible errors in the surface pressure field model is the difference between two variants of NCEP numerical weather models: the NCEP Reanalysis

and the NCEP Operational Final Analysis, although these two models are obviously not independent. The NCEP Operational Final Analysis model is an improved version with respect to an earlier model NCEP Reanalysis. The improved horizontal (1° instead of 2.5°) and vertical resolution (42 layers instead of 28) allows a better modeling of atmospheric dynamics. We computed station displacements due to atmospheric pressure loading using the NCEP Operational data set with a spatial resolution of 1.0° for the period from April 2002 to January 2003. The rms of the differences between the vertical and horizontal displacements computed with the NCEP Reanalysis and the NCEP Operational data are shown in the 6th and 7th columns of Table 1. Correlations between the differences and the modeled signal are shown in columns 8, 9. The mean error is about 10% for the vertical and horizontal components. It is noticeable that the differences are larger for stations enclosed by mountains, for example, Santiago. This is due to the fact that the 2.5° or even 1.0° spatial resolution of the NCEP Reanalysis and Operational data sets is not sufficient to model the topographic variations in mountainous areas and, therefore, the surface pressure variations. Our results are similar to conclusions made by *Velicogna et al.* [2001].
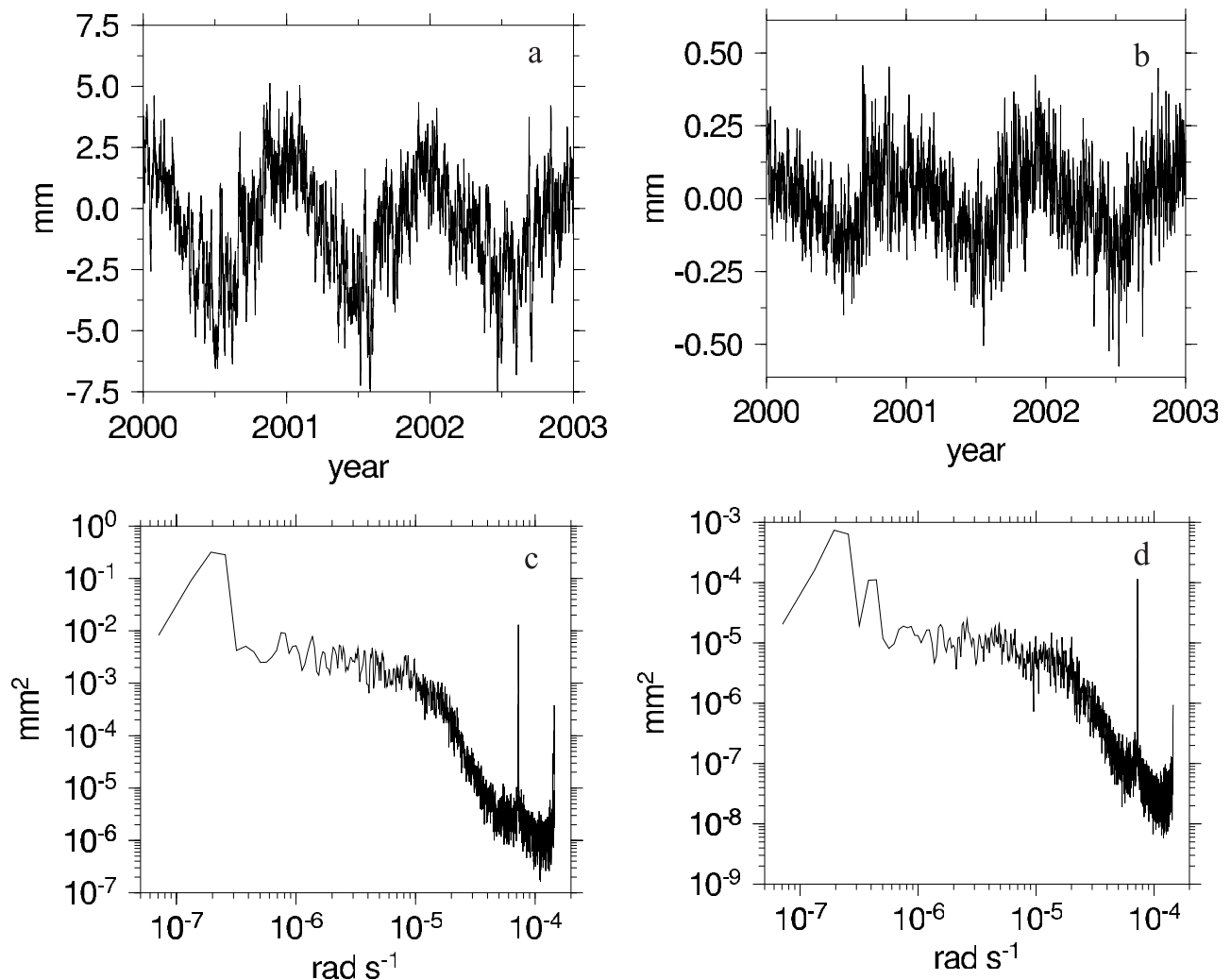
Figure 2. (a) Vertical and (b) east displacements induced by atmospheric pressure loading at the station Hartrao. Power spectrum of the (c) vertical and (d) east displacements.

The precision of computation of pressure loading displacements is worse for mountainous stations.

[23] In order to evaluate the errors caused by mismodeling of the ocean response, we compared ocean bottom pressure variations, as well as the induced loading effects, from two runs of the Coupled Large-Scale Ice Ocean (CLIO) general circulation model [*Goosse and Fichefet*, 1999]; the first one is forced by atmospheric pressure, surface winds and heat fluxes [*de Viron et al.*, 2002], and the other one is forced only by surface winds and heat fluxes, i.e., assuming an IB response. The differences between these two runs can therefore be interpreted as the departure of the ocean response from the IB assumption. We also validated the bottom pressure changes modeled by CLIO with measurements from the Global Undersea Pressure (GLOUP) data set (http://www.pol.ac.uk/psmslh/gloup/gloup.html) and found that the CLIO model agrees with the measurements of the bottom pressure at the level of 20%. We show in the 10th and 11th columns of Table 1 the ratio of the rms of these differences to the rms of our atmospheric loading series with the IB model for all stations, as well as a mean value of this ratio. Correlations between the differences and modeled signal

are shown in columns 12 and 13. Thus the mean vertical and horizontal errors are below 10% and 20% respectively. As expected, these values are higher for island stations (f.e., Kokee, Mk-vlba) or stations close to the coasts (Richmond, Hobart26, etc.), where the atmospheric loading itself is very small: rms below 1 mm and 0.5 mm for the vertical and horizontal components respectively.

[24] Table 2 summarizes the error budget. Combining all known sources of errors we evaluate the total uncertainty of our computation of site displacements due to atmospheric pressure loading to be 15%.

3. Validation of the Model Using VLBI Observations

[25] We selected VLBI for validation of our time series of atmospheric pressure loading. Each of the three main space geodetic techniques, GPS, SLR and VLBI, has its own advantages and disadvantages, although in general they are quite competitive. We chose VLBI because of the maturity of the VLBI data analysis technique. Complete reanalysis of the whole set of VLBI observations takes about a couple of

Table 1. Statistics of Displacements Caused by Atmospheric Pressure Loading and Statistics of the Differences in Time Series: NCEP Operational Versus NCEP Reanalysis Data Set and CLIO Model Versus IB Hypothesis

| Station	Lat., deg	Long., deg	Displacements		Operational/Reanalysis				CLIO/IB			
			rms (Vertical), mm	rms (Horizontal), mm	rms of Difference (Vertical), %	rms of Difference (Horizontal), %	Correlation (Vertical)	Correlation (Horizontal)	rms of Difference (Vertical), %	rms of Difference (Horizontal), %	Correlation (Vertical)	Correlation (Horizontal)
ALGOPARK	45.8	281.9	3.7	0.6	4.0	5.7	0.96	0.99	4.7	11.0	0.02	0.00
BR-VLBA	47.9	240.3	3.2	0.6	8.8	9.8	0.96	0.92	6.6	12.0	0.02	−0.08
DSS45	−35.2	149.0	2.5	0.4	5.8	9.1	0.97	0.90	9.0	13.1	0.03	−0.13
DSS65	40.2	355.7	2.6	0.6	8.2	12.7	0.97	0.77	7.6	15.0	0.08	0.02
FD-VLBA	30.5	256.1	2.4	0.4	10.4	9.4	0.93	0.95	9.2	19.1	−0.05	−0.07
FORTLEZA	−3.9	321.6	1.0	0.3	15.5	12.5	0.94	0.86	25.4	23.3	0.35	−0.07
GILCREEK	64.8	212.5	4.7	0.6	7.8	12.3	0.99	0.95	2.7	16.2	0.12	0.06
HARTRAO	−25.7	27.7	2.3	0.2	7.8	18.3	0.88	0.91	10.3	16.4	−0.01	0.04
HATCREEK	40.6	238.6	2.0	0.5	10.3	9.3	0.97	0.94	9.4	14.4	−0.04	−0.10
HAYSTACK	42.4	288.5	2.8	0.6	4.5	4.8	0.92	0.94	11.2	14.6	−0.01	0.06
HN-VLBA	42.7	288.0	3.0	0.6	4.5	5.2	0.92	0.96	6.6	19.6	0.02	0.04
HOBART26	−42.6	147.4	1.6	0.4	4.9	8.1	0.93	0.95	12.0	33.4	−0.05	−0.07
HRAS 085	30.5	256.0	2.4	0.4	10.4	9.4	0.93	0.95	9.2	19.1	0.01	−0.07
KASHIMA	35.8	140.7	1.2	0.6	7.4	6.0	0.96	0.93	17.3	30.2	0.11	0.00
KASHIM34	35.8	140.7	1.2	0.6	7.5	6.0	0.96	0.93	17.4	33.8	0.10	0.01
KAUAI	22.0	200.3	0.5	0.2	11.7	10.5	0.99	0.96	52.4	87.3	−0.09	0.06
KOKEE	22.0	200.3	0.5	0.2	11.7	10.5	0.99	0.96	52.4	89.9	−0.09	0.06
KP-VLBA	31.8	248.4	1.9	0.5	13.8	10.9	0.87	0.93	12.1	44.6	−0.09	−0.12
LA-VLBA	35.6	253.7	2.5	0.5	8.1	9.6	0.99	0.95	8.6	44.1	−0.07	−0.06
MATERA	40.5	16.7	2.3	0.8	9.9	8.7	0.92	0.75	9.1	40.5	−0.03	−0.03
MEDICINA	44.3	11.6	3.3	0.9	7.0	9.3	0.86	0.76	6.9	38.0	−0.01	−0.01
MK-VLBA	19.7	204.5	0.5	0.2	12.3	10.6	0.74	0.76	53.0	37.5	−0.12	0.03
MOJAVE12	35.2	243.1	1.9	0.5	12.4	11.7	0.85	0.89	11.4	60.6	−0.07	−0.11
NL-VLBA	41.6	268.4	3.6	0.7	4.3	6.1	0.96	0.94	5.7	44.5	0.03	−0.02
NOTO	36.7	15.0	1.4	0.7	12.9	11.2	0.98	0.77	13.6	62.2	−0.02	−0.03
NRAO20	38.2	280.2	3.0	0.5	6.5	7.1	0.92	0.97	6.8	58.1	0.04	0.03
NRAO85 3	38.2	280.2	3.0	0.5	6.5	7.1	0.92	0.97	6.8	60.6	0.04	0.03
NYALES20	78.9	11.9	1.8	0.7	6.7	7.0	0.60	0.83	5.8	62.6	0.03	−0.01
ONSALA60	57.2	11.9	4.7	1.1	2.8	4.5	0.60	0.77	4.7	27.1	−0.03	−0.00
OV-VLBA	37.0	241.7	2.0	0.5	12.7	10.9	0.88	0.91	10.1	28.6	−0.06	−0.11
OVRO 130	37.0	241.7	2.0	0.5	12.9	10.9	0.87	0.91	10.1	33.8	−0.06	−0.11
PIETOWN	34.1	251.9	2.3	0.4	9.8	10.4	0.90	0.93	8.8	40.3	−0.07	−0.08
RICHMOND	25.5	279.6	0.9	0.4	7.9	6.1	0.81	0.86	26.5	47.6	−0.03	0.02
SANTIA12	−33.0	289.3	1.4	0.4	15.7	16.0	0.52	0.73	15.7	44.6	0.18	−0.04
SC-VLBA	17.6	295.4	0.5	0.3	15.7	10.0	0.89	0.85	55.9	44.6	0.10	0.00
SESHAN25	30.9	121.2	3.5	0.9	7.6	7.8	0.77	0.85	7.1	34.0	0.03	0.01
TSUKUB32	35.9	140.1	1.4	0.5	7.0	6.9	0.95	0.90	14.4	31.2	0.11	0.01
VNDNBERG	34.4	239.4	1.0	0.4	8.3	8.8	0.87	0.91	19.8	30.2	−0.08	−0.12
WESTFORD	42.4	288.5	2.8	0.6	4.5	4.8	0.92	0.94	7.7	31.7	0.02	0.04
WETTZELL	49.0	12.9	4.9	0.9	4.2	6.4	0.77	0.80	16.9	28.3	−0.03	0.04
Mean			**2.6**	**0.6**	**8.7**	**9.1**	**0.89**	**0.89**	**15.2**	**39.1**	**0.01**	**−0.02**
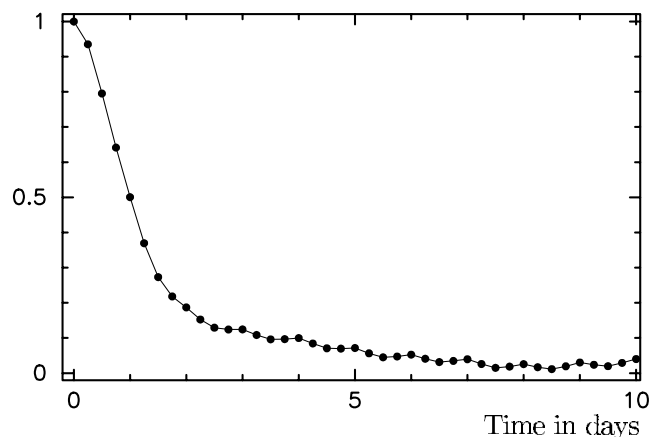
Figure 3. Temporal autocorrelation of the vertical component of the atmospheric pressure loading at the station Algopark.

Figure 5. Map of VLBI stations used in the analysis.

hours on rather a modest computer. Therefore the consistency of reduction models and parameter estimation can easily be enforced. These factors make VLBI attractive for investigating tiny effects like atmospheric pressure loading.

3.1. Observations

[26] All dual-band Mark-3/Mark-4/K-4 VLBI observations carried out under various geodetic and astrometric programs from 1979 to the present are available on-line at the International VLBI Service for Geodesy and Astrometry (IVS) Data Center at http://ivscc.gsfc.nasa.gov [*Vandenberg*, 1999] (available at http://ivscc.gsfc.nasa.gov/publications/ar1999). The VLBI data set has substantial spatial and time inhomogeneity. Typically, observations are made in sessions with a duration of about 24 hours. Observations were sporadic in the early 80s, but in January 1984 a regular VLBI campaign for the determination of EOP started first with 5 day intervals, from May 1993 with weekly intervals, and from 1997 twice per week. In addition to the observations dedicated to EOP measurements, various other observing campaigns were running. On average 150 sessions per year have been observed since 1984.

[27] In total 144 stations participated in observations, although a majority of them observed only during short cam-
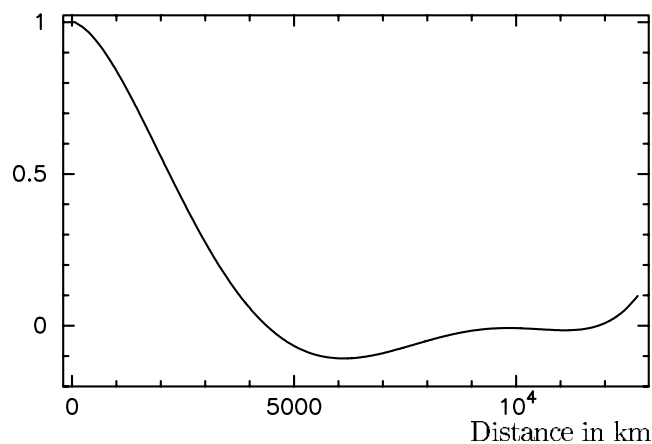
paigns. The stations which participated in more than 20,000 observations for more than three years were used for analysis. Forty-six stations satisfied these criteria. Four stations which participated in the Key Stone Project (KSP) [*Takahashi et al.*, 2000], Kashim11, Koganei, Miura, Tateyama, were excluded since they observed mainly in a small local network, as well as two other stations, Crimea, because it had bad performance, and Ylow7296, since its sensitivity was too low. Only observations on the baselines between the 40 strong selected stations were used, and other observations (~6%) were discarded. Sessions with less than 3 strong stations were discarded entirely. Remaining were 3073 sessions from April 1980 to December 2002 with more than 3.5 million observations, and they were used in the analysis.

[28] The number of participating stations in each individual session varies from 2 to 20, although 4–7 is a typical number. No station participated in all sessions, but every station participated in sessions with many different networks. All networks have common nodes and, therefore, are tied together. Networks vary significantly, but more than 70% of them have a size exceeding the Earth's radius.

3.2. Choice of Parameterization

[29] The scatter of daily estimates of site positions is greater by a factor of 2–5 than the rms of atmospheric pressure loading displacements. Therefore we cannot directly see the signal in the site position time series. Besides, in order to resolve rank deficiency of the problem of simultaneous adjustment of coordinates of all site and EOP, net-rotation and net-translation constraints should be applied or an equivalent technique should be used. As a result adjustments of site positions become linearly dependent. Since only a small number of stations participates in a typical VLBI experiment, the influence of position variations of other observing stations of the network on position variations of a station of interest is not diluted to a

Figure 4. Smoothed spatial autocorrelation of the vertical component of the atmospheric pressure loading.

Table 2. Global Budget of the Errors of Computation of the Atmospheric Pressure Loading Displacements

Error Source	rms, %	Correlation
Numerical evaluation of the integral	1	0.0?
Green's function	<2	±1.0
Land sea mask	<5	0.7
Surface pressure field	10	0.9
Ocean response	10	0.0
Total	**15**	

negligible level. It makes the interpretation of daily VLBI site position time series uncertain.

[30] One of the ways to assess validity of the model is to compute two time series of baseline lengths: the first with applying the atmospheric pressure loading model and the second without applying the model. Baseline lengths are invariant with respect to a rotation and translation and, therefore, net-translation and net-rotation constraints do not affect them. We introduce the reduction of variance coefficient R:

$$R = \frac{\Delta\sigma^2 + \sigma_m^2}{2\sigma_m^2}, \tag{7}$$

where $\Delta\sigma^2$ is the difference between the mean square of baseline length residuals before and after applying the model, and σ_m^2 is the variance of the signal in the model. If the model is perfect and the signal under consideration is not correlated with another unmodeled effects, the coefficient is 1. If the baseline length series does not contain the signal coherent with the model at all, then applying the model increases the variance by the amount of the variance of the signal in that model, and the coefficient of reduction of variance is 0. We should emphasize the importance of the assumption of the lack of correlation between the pressure loading signal and noise: we can extract the signal which is below the noise level if, and only if, some additional information about the noise is exploited. The validity of this assumption is based on the fact that as can bee seen in Figures 1 and 2, the spectrum of the atmosphere pressure loading at frequencies below one day is flat, except for a peak at the annual frequency for some stations. Thus the atmospheric pressure loading can be considered to some degree as a stochastic Gaussian process. The spectrum of the VLBI residuals is also flat. Therefore our condition of lack of correlation between the atmosphere pressure loading series and residual unmodeled effects is fulfilled if an unmodeled contribution to VLBI delay and pressure loading are independent.

[31] Although this approach gives us a quantitative measure of the adequacy of the model, it has some disadvantages. It lets us determine only the reduction of variance coefficients for the projection of the difference of the site displacements vectors on the baseline vector instead of the coefficients for each site and each component independently.

[32] Another approach is to represent the atmospheric pressure loading signal as a product $A \cdot a_m$, where a_m is the modeled signal, and to estimate directly from the VLBI time delays the unknown parameter A which hereafter we call admittance factor between the modeled signal and the observables. It can easily be verified that if A is the only estimated parameter and the modeled signal is not correlated with an unmodeled contribution to the observable, then the expectation of the LSQ estimate of the admittance factor, $E(\hat{A})$, is

$$E\left(\hat{A}\right) = \rho\frac{\sigma_l}{\sigma_m}, \tag{8}$$

where ρ is the correlation coefficient between modeled and true atmospheric pressure loading, and σ_l^2 is the variance of

the true pressure loading. Under the same assumption the reduction of variance $\Delta\sigma^2 = (2E(\hat{A}) - 1)\,\sigma_m^2$ and therefore, the coefficient of reduction of variance R is equal to $E(\hat{A})$. If other parameters are adjusted in addition to A, this property is preserved at the level of correlations between $\hat{A}$ and the estimates of other parameters. The admittance factor A shows how much of the power of the modeled signal is present in the observables.

3.3. Estimation Model

[33] We made solutions of two classes: global solutions, in which we estimated the positions and velocities of all sites over the entire data set, and baseline solutions, in which we estimated site positions for each VLBI experiment independently using ionosphere free linear combination of group delays at S and X bands. Estimated parameters were split into two classes: basic parameters, which are usually adjusted in processing VLBI experiments, and specific parameters of interest. Basic parameters belong to one of the following three groups: (1) global (over the entire data set), containing positions of 511 primary sources and proper motions of 79 sources; (2) local (over each session), containing pole coordinates and their rates, UT1, UT1 rate, positions of other sources, azimuthal troposphere path delay gradients for all stations and their rates, station-dependent clocks modeled by second-order polynomials, and baseline-dependent clock offsets; and (3) segmented (over 0.33–1.0 hours), containing coefficients of a linear spline which models atmospheric path delay (0.33 hour segment) and clock function (1 hour segment) for each station. The estimates of clock function absorb uncalibrated instrumental delays in the data acquisition system.

[34] The rate of change of atmospheric path delay and clock function between two adjacent segments was constrained to zero with weights reciprocal to 40 psec/hour and 2×10^{-14} sec/sec, respectively, in order to stabilize solutions. No-net-translation and no-net-rotation constraints were imposed on the adjustments of site positions and velocities as well as no-net-rotation constraints were imposed on adjustments of source positions in order to solve the LSQ problem of incomplete rank.

[35] A pair of baseline solutions was made with only basic parameters estimated and station positions treated as local parameters. In reference solution B1 the atmospheric pressure loading time series was not applied; in solution B2 the contribution due to the model of atmospheric pressure loading was added to the theoretical model of the observables.

[36] In solutions G1, G5, G6 and G7 the list of global parameters included site positions, site velocities and overall admittance factors for the Up, East and North components of the modeled atmospheric pressure loading signal for all sites combined. In solution G2 we estimated the set of the admittance factors for the Up, East and North components for each station independently, and other parameters were the same as in the G1 solution.

[37] It should be noted that unlike estimation of positions of all stations, estimation of the Up, East and North admittance factors for all stations of a global network does not result in a rank deficiency. A partial derivative of time delay τ with respect to the admittance factor of the ith station is given by $(\partial\tau/\partial A_i) = (\partial\tau/\partial r_i)\,a_{mi}$, where r_i is a vector of station

Table 3. Global Admittance Factors

Solution	Up	East	North
G1	0.95 ± 0.02	1.17 ± 0.06	0.83 ± 0.07
G5	0.46 ± 0.09	1.08 ± 0.26	−0.89 ± 0.26
G6	0.98 ± 0.02	1.20 ± 0.06	1.02 ± 0.07
G7	0.88 ± 0.02		

coordinates. As was shown in Figure 3, the correlation between the atmosphere pressure loading at different stations is less than 0.1 at distances greater than 4000 km.

3.4. Theoretical Model

[38] The computation of theoretical time delays, with some exceptions, generally follows the procedure outlined in the IERS Conventions [*McCarthy*, 1996] and described in more detail by *Sovers et al.* [1998]. The GOT00 model [*Ray*, 1999] of diurnal and semidiurnal ocean tides, the NAO99 model [*Matsumoto et al.*, 2000] of ocean zonal tides, the equilibrium model of the pole tide and the tide with period of 18.6 years were used for the computation of displacements due to ocean loading. The hydrology model of *Milly and Shmakin* [2002a, 2002b] was used for the computation of displacements due to hydrology loading (D. S. MacMillan and J.-P. Boy, manuscript in preparation, 2004; D. S. MacMillan, personal communication, 2003). The empirical model of high-frequency Earth orientation parameters derived from analysis of the VLBI data [*Petrov*, 2000a] (available at http://aa.usno.navy.mil/colloq180/Proceedings) and the IERS96 semiempirical nutation expansion were used. The *Niell* [1996] mapping functions were used for modeling and estimating the tropospheric path delay. The displacement of the reference point of a VLBI station due to thermal expansion of the antenna was not modeled. Although *Nothnagel et al.* [1995] proposed a model for an antenna's thermal expansion, attempts to validate this model were not successful. We did not include the model of nontidal ocean loading, because this effect is one order of magnitude smaller than the atmosphere pressure loading, and it has not been fully investigated. It will be considered in a future paper.

4. Discussion

4.1. Analysis of Global Admittance Factors

[39] Table 3 shows admittance factors determined in solution G1. The uncertainties of the results were derived by propagating the group delay errors. These errors were computed on the basis of the signal to noise ratio of the cross correlation function of the recorded signal from the receivers and the empirical baseline-dependent reweighting parameters which, being added in quadrature to the uncertainties of group delays, made the χ^2/f of the postfit residuals close to unity. In addition to that, the formal uncertainties were scaled by a factor of 1.5. Numerous tests of splitting the data set into subsets in time and in space showed that the VLBI formal uncertainties are underestimated by a factor of 1.5. The origin of this discrepancy is not completely understood, but there are indications that it may be caused by fringe phase variations due to instrumental errors [*Petrov*, 2000b] (available at http://ivscc.gsfc.nasa.gov/publications/gm2002).

[40] Above we showed the estimates of the rms of possible errors in our computation of atmospheric pressure loading and their correlations with the modeled signal. Assuming that

the different error sources a) are not correlated with each other, b) are small with respect to the signal, we can present the expectation of the admittance factor in this form:

$$E(A) = 1 - \sum k_i r_i + \sum k_i^2 \left(2r_i^2 - 1\right) + 4 \sum \sum_{i \neq j} k_i k_j r_i r_j + O\left(k^3\right), \qquad (9)$$

where k is the ratio of the rms of errors to the rms of the modeled signal, r is the correlation between the error and modeled signal. The summing is done over all considered sources of errors.

[41] Using numerical values for r_i and k_i listed in Table 2, we evaluate the expectation of A: 0.90. Our estimates of the admittance factors are close to this value. This means that the known deficiency of the model is sufficient to explain the small deviation of the estimates of the global admittance factors from 1.

[42] Since the typical spectrum of atmospheric pressure loading shows peaks at semidiurnal (1.46×10^{-4} rad/s), diurnal (7.29×10^{-5}), semiannual (3.98×10^{-7} rad/s) and annual frequencies (1.99×10^{-7} rad/s) (Figures 1 and 2), we would like to see how applying the atmospheric pressure loading model affects residual harmonic site position variations at these frequencies. In order to assess this effect, we made two solutions, G3 and G4, and estimated the sine and cosine amplitudes of position variations of all sites at 32 tidal frequencies, including these four frequencies with noticeable atmospheric pressure loading signal. Atmospheric pressure loading was applied in solution G4, but was not in solution G3. Amplitudes at the frequencies of diurnal, semidiurnal and long period bands where no tidal signal is expected were estimated as well in order to calibrate the uncertainties of the results. The ratio of the weighted sum of squares of the residual amplitudes over all stations at the specific frequency to its mathematical expectation, $\mathcal{P}$, was used as a measure of the power of the residual signal. In the absence of the signal these statistics should be less than 1.25 at the 95% confidence level. Therefore large values of $\mathcal{P}$ which exceed this limit indicate the presence of the residual signal. This technique is explained in more details by *Petrov and Ma* [2003].

[43] Table 4 shows the estimates of $\mathcal{P}$ for each of the four frequencies of interest. We see that applying the model of atmospheric pressure loading reduces the amplitude of the residual signal at semidiurnal and semiannual frequencies, but noticeably increases the amplitude at the annual frequency. In all cases the power of remaining residual signal is still significant. This table shows us that the atmosphere pressure loading is not the dominating source of observed residual harmonic site position variations at these frequencies.

[44] The presence of the narrow-band residual signal to some degree violates the assumption of lack of correlations which was put at the basis of the agreement test. Two harmonic signals may be independent and correlated. In order to investigate the effect of the atmospheric pressure loading signal at the annual frequency, the frequency with the largest harmonic signal, we passed the pressure loading time series through a narrow-band filter with a passing window around the annual frequency: $1.79 \times 10^{-7}, 2.19 \times 10^{-7}$ rad/s. We made two solutions, G5 in which we estimated the global admittance factor of the annual constituent of the

Table 4. Ratio of the Weighted Sum of Squares of the Estimates of Residual Amplitudes of Harmonic Site Position Variations Without Applying the Model of Atmospheric Pressure Loading and After Applying the Model

Wave	Without Model		With Model	
	Vertical	Horizontal	Vertical	Horizontal
Semidiurnal	2.77	1.73	2.35	1.58
Diurnal	4.26	2.31	4.33	2.25
Semiannual	2.77	1.07	2.31	1.10
Annual	5.18	2.45	6.00	2.45

atmospheric pressure loading and solution G6 in which we estimated the global admittance factor with the signal at the annual band removed. The results are presented in Table 3. The admittance factor in solution G6 increased by 3%. It gives us a measure of the distortion of the statistical tests caused by unaccounted correlations between the annual narrow-band unmodeled signal and atmospheric pressure loading. Similar results were reported by VDH who noted that removal of the annual signal from the atmospheric pressure loading increased variance reduction of the baseline length series.

[45] The fact that modeling atmospheric pressure loading increases the level of the residual signal at annual frequency does not necessarily mean that the model is wrong. If two anticorrelated signals contribute to the observables, then including the model of only one of the signals in the procedure of reduction of observations may result in increasing variance, even if the model is perfect. We know that various phenomena may contribute to the annual site position variation, such as hydrological signal, nontidal ocean loading, thermal antenna deformation, mismodeling troposphere path delay, etc., and atmospheric pressure loading is not the greatest contributor. It should be noted that this means that a reduction of the variance coefficient and an admittance factor cannot be considered as a valid test of goodness of the model in this specific case.

[46] We should acknowledge that currently we are unable to test directly whether the annual constituent of the atmospheric pressure loading signal is modeled correctly or not. It will be possible in the future when a complete model of site position variations will be built and the power of the residual signal will become less than the power of annual pressure loading signal. Although attempts to model seasonal effects show certain improvement [*Dong et al.*, 2002], we are still far from a solution of this problem.

[47] At the same time the admittance factor for the vertical displacements is close to unity at the level of measurement noise for the wide-band component of the modeled displacements due to atmosphere pressure loading after subtraction of the annual component. It provides us indirect evidence that we have modeled atmosphere pressure loading correctly at the annual frequency as well, since the Green's function and land-sea mask are frequency-independent, and our estimate of the error budget set the upper limit of possible seasonal errors of the atmosphere pressure field.

4.2. Analysis of Admittance Factors for Individual Stations

[48] Although we concluded in the previous section that the average admittance factor is very close to unity, it does not necessarily mean that the admittance factors are close to unity

for each individual station. Table 5 shows the estimates of the admittance factors from the G2 solution. The estimates with the formal uncertainties greater than 0.5 are omitted in the table. It is not surprising that the admittance factor of the Kokee station is far from unity, even negative, since the station is located on an island in the middle of the Pacific ocean. It is more surprising that the admittance factors at the Hn-vlba and Westford stations are so different, since the distance between these stations is only 54 km and, indeed, the time series of the pressure loading are very similar. We suspect some problem with data at the station of Hn-vlba. Low admittance at the La-vlba and Pietown stations located in mountainous regions may be explained by greater errors in the model of surface pressure. We do not have explanation of the negative admittance factor at the station of Ov-vlba. Another peculiarity is the anomalously high admittance factors at the Seshan25 and Tsukub32 stations. It is known that the response of the Yellow Sea to tidal forcing is amplified by 10 times, and a significant nonlinear M_4 tide is observed [*Lefèvre et al.*, 2000]. We can expect that the response to atmospheric forcing will be also substantially nonlinear and not consistent with the IB hypothesis.

4.3. Analysis of Reduction of Variance Coefficients

[49] In order to compare our results with the early VDH paper, we performed our analysis in a manner similar to that used in the analysis of those authors. We computed the time series of baseline lengths in the B1 and B2 solutions. A linear model was fit in the series with discontinuities at epochs of seismic events for several stations. The weighted root mean square of residual baseline lengths was computed for all baselines with more than 100 sessions for both the B1 and B2 solutions. Sixty-nine baselines satisfy this criterion. The coefficients of reduction of variance were computed using baseline length variances.

[50] The histogram of the distribution of the coefficients of reduction of variance is presented in Figure 6. The weighted mean value $\bar{R}$ over 69 baselines is 0.97 ± 0.04. For the computation of the uncertainty of the mean value we used the variance of R which can easily be derived from the results presented in the appendix of VDH:

$$\text{var}(R) = \frac{\sigma_1^2 + \sigma_2^2 - \sigma_m^2}{2(N-1)\sigma_m^2}, \tag{10}$$

where σ_1^2 and σ_2^2 are the mean squares of the baseline length residuals of solutions B1 and B2 respectively, σ_m^2 is the mean square of the modeled baseline changes with respect to the mean value computed over the period of time of VLBI observation, N is the number of observing sessions.

[51] VDH analyzed 22 baselines for the period 1979 to 1992. They reported a much lower value of the reduction of variance coefficient, 0.62, which means that 38% of the power of the signal in their series of atmospheric pressure loading is not present in the VLBI data. In order to check whether the differences may be due to changes in the quality of VLBI data collected after 1992 we restricted our calculations to exactly the same set of observations and baselines used by VDH. We got 1.10 ± 0.10 for the coefficient of reduction of variance for this case. It deviates at the 3σ level from the value reported by VDH. The differences in our analysis technique of VLBI observations and the technique of VDH are not significant enough to explain this large

Table 5. Admittance Factors From G2 Solution

Station	Up	East	North
ALGOPARK	1.14 ± 0.09	1.03 ± 0.18	0.82 ± 0.21
BR-VLBA	0.75 ± 0.07	1.11 ± 0.13	0.42 ± 0.12
DSS45	0.85 ± 0.40		
DSS65	2.30 ± 0.34		
FD-VLBA	1.35 ± 0.07	2.44 ± 0.18	1.03 ± 0.13
FORTLEZA	1.08 ± 0.46		
GILCREEK	0.94 ± 0.03	1.18 ± 0.11	0.35 ± 0.15
HARTRAO	1.53 ± 0.33		
HAYSTACK	1.00 ± 0.36		
HN-VLBA	0.12 ± 0.11	1.09 ± 0.16	1.03 ± 0.18
HRAS 085	1.84 ± 0.39		
KOKEE	−0.95 ± 0.37		
KP-VLBA	0.92 ± 0.11	0.33 ± 0.19	0.07 ± 0.14
LA-VLBA	0.36 ± 0.06	1.33 ± 0.15	0.68 ± 0.12
MATERA	0.79 ± 0.15	0.12 ± 0.28	1.17 ± 0.22
MEDICINA	0.67 ± 0.12	0.15 ± 0.25	1.20 ± 0.19
MOJAVE12	0.89 ± 0.24	1.93 ± 0.39	0.23 ± 0.38
NL-VLBA	0.91 ± 0.05	1.80 ± 0.10	0.61 ± 0.11
NRAO20	1.41 ± 0.08	1.99 ± 0.23	0.07 ± 0.21
NRAO85 3	1.56 ± 0.16	1.61 ± 0.42	0.67 ± 0.35
NYALES20	0.69 ± 0.12	0.60 ± 0.14	1.56 ± 0.18
ONSALA60	0.27 ± 0.08	1.03 ± 0.12	1.59 ± 0.13
OV-VLBA	−0.73 ± 0.11	0.94 ± 0.16	0.34 ± 0.15
PIETOWN	0.12 ± 0.07	1.18 ± 0.17	0.35 ± 0.13
SESHAN25	4.03 ± 0.39		
TSUKUB32	3.91 ± 0.38		
WESTFORD	1.22 ± 0.06	0.68 ± 0.11	0.06 ± 0.13
WETTZELL	1.14 ± 0.04	0.55 ± 0.12	0.91 ± 0.10

discrepancy. So, the differences in the reduction of variance coefficients come from the differences between the series of the atmospheric pressure loading displacements. First, the predicted baseline loading effects of VDH and *vanDam et al.* [1994] suffered from the problem that they have the wrong sign for the horizontal deformation in the North direction (T. vanDam, personal communication, 2003). Second, we used the NCEP Reanalysis model, but VDH used an older model: the National Meteorological Center operational model with a 12 hour resolution. Third, we used a land-sea mask with a resolution of $0.25° \times 0.25°$: ten times better then the resolution of the surface pressure model. As shown in section 2.2, this difference alone can cause an error in the vertical displacements as large as 10%. Fourth, we used a different numerical algorithm for computing the convolution integral.

4.4. Application of the Pressure Loading Model to Data Reduction

[52] In the past, several authors recommended finding the linear regression of the vertical atmospheric pressure loading and local surface pressure and using this simple model in operational data analysis. *Rabbel and Zschau* [1985, p. 83] warned that since "the magnitude of the displacements is critically dependent on the spatial extension of the pressure distribution...there cannot be any unique regression coefficient between local displacements and local air pressure changes which could be used to correct geodynamics measurements for air-pressure-induced surface displacements." However, this simple model was used in the 20th century. In order to evaluate the errors of this approach, we computed coefficients of linear regression between the 22 year long time series of the displacements caused by atmospheric pressure loading and local pressure at the station obtained by interpolation

of the NCEP surface pressure field. Using these regression coefficients we computed a synthetic time series of the pressure loading for each station and estimated the admittance factors of these time series in solution G7. The results are shown in Table 3. We see that the simple regression model works surprisingly well for vertical components. This test shows that the amount of the power of the signal which is present in the model, but is not present in the data, is increased from 5% to 12% when a regression model is used.

[53] Currently, there is no need to resort to a simplified linear regression. Numerical weather models are available on-line promptly, and a computation of a 20 years long series of pressure loading for all VLBI and SLR sites takes only several days at a personal computer using the efficient algorithm presented in Appendix A.

[54] Applying atmospheric pressure loading in a procedure of data reduction causes a small change in the resulting terrestrial reference frame: the maximum site position change among the stations which observed one year or longer is 2 mm, the velocity change is typically below 0.1 mm/yr with the maximum change of 0.4 mm/yr, and the scale factor is increased by 0.05 ± 0.02 ppb. Taking into account the horizontal component of the displacement due to atmospheric pressure loading causes rms differences in the estimates of polar motion and UT1 at the level of 100 prad and differences in the estimates of nutation angles with an rms of 30 prad. The uncertainties of the EOP derived from processing daily VLBI sessions are currently at the level of 200–400 prad. Therefore omission of the horizontal atmospheric pressure loading is currently not a significant source of noise in the estimates of the EOP.

5. Conclusions

[55] We found that vertical and horizontal displacements caused by atmospheric pressure loading currently can be computed with errors less than 15% by convolution of the surface pressure field from the NCEP Reanalysis model with Green's functions. Our analysis of VLBI observations of 40 strong stations for the time period from 1980 till 2002 demonstrates that on average only 5% of the power of the modeled vertical pressure loading signal, 16% of horizontal signal and 3% of the signal in baseline lengths is not found in VLBI data. Thus all discrepancies between the observa-
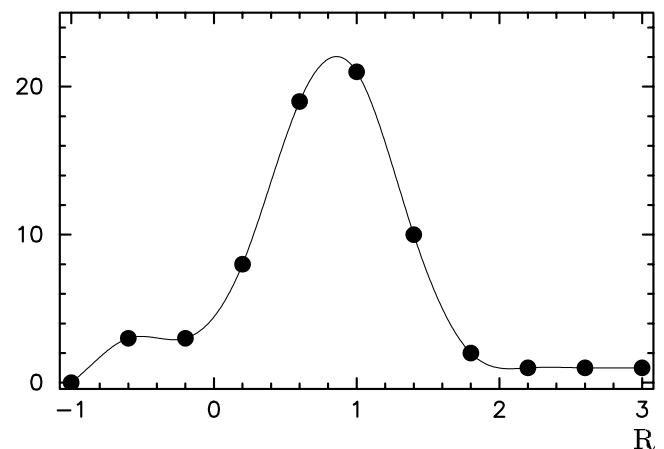

Figure 6. Histogram of the distribution of the reduction of variance coefficients.

tions and the model can be explained by known deficiencies of the model.

[56] Admittance factors of the time series of pressure loading vertical displacements without the annual constituent do not deviate from unity by more than the formal uncertainty. It means that at the confidence level of 5% the modeled signal is completely recovered from the VLBI observables. This estimate sets the upper limit of possible errors in Green's functions: 4% for the radial Green's function and 12% for the horizontal Green's function.

[57] This allows us to conclude that on average our model of the displacements caused by atmospheric pressure loading is correct. At the same time for some stations the model does not agree with data perfectly. These stations are located either close to a coast, or in isolated islands, or in mountain regions. In the first case, poor modeling of the ocean response to atmospheric pressure forcing becomes a significant factor; in the latter case the spatial resolution of the weather model, $2.5° \times 2.5°$, is too coarse to represent adequately the surface pressure field variations.

[58] We have detected for the first time the horizontal component of the atmospheric pressure loading signal. This signal has never been before taken into account in routine reduction of geodetic observations. If not modeled, it adds noise to the horizontal site position with an rms of 0.6 mm and to the estimates of the EOP with an rms of 100 prad. According to the estimates of the error budget, the residual site displacements due to atmospheric pressure loading which are not accounted for by our model, on average have an rms of 0.4 mm for the vertical component and 0.1 mm for the horizontal component.

[59] The model presented here shows a significant improvement with respect to the previous models. The amount of power which is present in the model, but not found in the data is 38% for the VDH model, 12% when the linear regression approach is used, and 5% for our model.

[60] We propose our model of the atmospheric pressure loading for use in routine processing of space geodesy observations. We have computed time series of the atmospheric pressure loading for all VLBI and SLR sites starting from May 1976. These time series are available on the Web at http://gemini.gsfc.nasa.gov/aplo and are updated daily. Since December 2002 the contribution of the atmospheric pressure loading displacements is applied on a routine basis at the VLBI analysis center of the NASA Goddard Space Flight Center.

[61] We expect that the new numerical weather models with higher spatial and temporal resolution will improve the agreement of pressure loading time series with observations in mountainous regions. Development of ocean models forced by atmospheric pressure and winds will improve the pressure loading estimates for coastal and island stations.

Appendix A: Algorithm for the Computation of Displacements Due to Atmospheric Pressure Loading

[62] We represent each component of the displacement as a sum of the contribution of the convolution integral over the land and over the ocean:

$$u(\vec{r},t) = u_{\mathrm{L}}(\vec{r},t) + \Delta\bar{P}_o(t)\, u_o, \qquad (A1)$$

where $\Delta\bar{P}_o(t)$ is the uniform sea floor pressure, $u_{\mathrm{L}}(\vec{r},t)$, $u_o(\vec{r})$ are

$$u_{\mathrm{L}}(\vec{r},t) = \sum_{i=1}^{n}\sum_{j=1}^{m} \Delta P(\vec{r}_{ij}',t)\, q(\vec{r},\vec{r}_{ij}')\cos\varphi_i \iint_{cell_{ij}} G\big(\psi(\vec{r},\vec{r}_{ij}')\big)ds$$

$$u_o(\vec{r}) = \sum_{i=1}^{n}\sum_{j=1}^{m} q(\vec{r},\vec{r}_{ij}')\cos\varphi_i \iint_{cell_{ij}} G\big(\psi(\vec{r},\vec{r}_{ij}')\big)ds, \qquad (A2)$$

and index i runs over latitude and index j runs over longitude. Here we replaced the integration over the sphere with a sum of integrals over small cells. $q = 1$ for the vertical component.

[63] Green's functions have a singularity in 0, so care must be taken in using numerical schemes for computing the convolution integral. Although the Green's function cannot be represented analytically over the whole range of its argument, we can always find a good approximation over a small range. We approximate the function $G(\psi)\cdot\psi$ by a polynomial of the third degree $\alpha + \beta\psi + \gamma\psi^2 + \delta\psi^3$. In order to compute the integral (A2) over the cell, we introduce a two-dimensional Cartesian coordinate system with the origin in the center of the cell and the axis x toward east, the axis y toward north. We neglect the Earth's curvature and consider the cell as a rectangle with borders $[-a, a]$, $[-b, b]$ on the x and y axes respectively. Then the integral of the Green's function over the cell with respect to a site with coordinates (x_s, y_s) is evaluated analytically:

$$\iint_{cell} G(\psi(x_s,y_s))ds$$

$$= \int_{-b-a}^{b}\int^{a} \left(\frac{\alpha}{\sqrt{x^2+y^2}} + \beta + \gamma\sqrt{x^2+y^2} + \delta(x^2+y^2) \right) dx\,dy$$

$$= \left(\alpha y_2 + \frac{\gamma}{6}y_2^3\right)\ln\frac{x_2+z_{22}}{x_1+z_{12}} - \left(\alpha y_1 + \frac{\gamma}{6}y_1^3\right)\ln\frac{x_2+z_{21}}{x_1+z_{11}}$$

$$+ \left(\alpha x_2 + \frac{\gamma}{6}x_2^3\right)\ln\frac{y_2+z_{22}}{y_1+z_{21}} - \left(\alpha x_1 + \frac{\gamma}{6}x_1^3\right)\ln\frac{y_2+z_{12}}{y_1+z_{11}}$$

$$+ (y_2-y_1)(x_2-x_1)\left[\beta + \frac{\delta}{3}\left(z_{11}^2 + z_{22}^2 + x_1 x_2 + y_1 y_2\right)\right] \quad (A3)$$

$$+ \frac{\gamma}{3}[x_2(y_2 z_{22} - y_1 z_{21}) - x_1(y_2 z_{12} - y_1 z_{11})];$$

$$x_1 = -a - x_s; \qquad x_2 = a - x_s;$$
$$y_1 = -b - y_s; \qquad y_2 = b - y_s;$$
$$z_{11} = \sqrt{x_1^2 + y_1^2}; \qquad z_{12} = \sqrt{x_1^2 + y_2^2};$$
$$z_{21} = \sqrt{x_2^2 + y_1^2}; \qquad z_{22} = \sqrt{x_2^2 + y_2^2}.$$

Coordinates x_s, y_s are computed as

$$x_s = \vec{E}(\vec{r}_{ij}')\cdot\vec{T}(\vec{r}_{ij}',\vec{r}) \qquad y_s = \vec{N}(\vec{r}_{ij}')\cdot\vec{T}(\vec{r}_{ij}',\vec{r}), \qquad (A4)$$

where $\vec{T}(\vec{r}_{ij}',\vec{r})$ is

$$\vec{T}(\vec{r}_{ij}',\vec{r}) = \frac{\vec{r}_{ij}' \times \left[\vec{r}\times\vec{r}_{ij}'\right]}{\left|\vec{r}_{ij}' \times \left[\vec{r}\times\vec{r}_{ij}'\right]\right|} \qquad (A5)$$

and $\vec{E}(\vec{r}'_{ij})$, $\vec{N}(\vec{r}'_{ij})$ are unit vectors in east and north direction with respect to the center of the cell:

$$\vec{E}(\vec{r}'_{ij}) = \begin{pmatrix} \sin\lambda' \\ \cos\lambda' \\ 0 \end{pmatrix} \qquad \vec{N}(\vec{r}'_{ij}) = \begin{pmatrix} \sin\varphi'\cos\lambda' \\ -\sin\varphi'\sin\lambda' \\ \cos\varphi' \end{pmatrix}.$$

(A6)

[64] We found that when the coefficients $\alpha(\psi)$, $\beta(\psi)$, $\gamma(\psi)$ and $\delta(\psi)$ are computed with the step 0.002 rad over the range [0, 0.16] rad, and with the step 0.02 rad over the range [0.16, π], the error of the approximation of the integral (A3) for a cell of size 0.044 rad (2.5°) does not exceed 1%. At large angular distances we can consider the Green's function to be constant over the cell. For an angular distance more than 0.16 rad, taking the Green's function out of the integral (A2) and replacing it with the value at the angular distance between the site and the center of the cell causes an error of less than 1%.

[65] Two land-sea masks are used for practical computation: coarse with the resolution of the surface pressure grid, and fine. If the cell of the coarse land-sea mask is completely land or completely sea, this cell is used for computing the integral (A3). Otherwise, the coarse resolution cell is subdivided in smaller cells of the fine resolution grid, and the integral over each fine resolution cell is computed independently. The surface pressure is considered as defined at the corners of the coarse resolution cell. The pressure at the center of the cell is obtained by bilinear interpolation. When $u_L(\vec{r})$ is computed, the cells which are over ocean are bypassed. Alternatively, the cells which are over land are bypassed when $u_o(\vec{r})$ is computed.

[66] The computation of horizontal vectors is done separately for north and east components. The north and east components of the vector $\vec{q}(\vec{r}, \vec{r}')$ are

$$q_N(\vec{r}, \vec{r}') = -\vec{T}(\vec{r}, \vec{r}') \cdot \vec{N}(\vec{r})$$
$$q_E(\vec{r}, \vec{r}') = -\vec{T}(\vec{r}, \vec{r}') \cdot \vec{E}(\vec{r}),$$

(A7)

where $\vec{T}(\vec{r}, \vec{r}')$ is defined in a way similar to equation (A5), but with the reverse order of arguments, $\vec{E}(\vec{r})$, $\vec{N}(\vec{r})$ are defined according to equation (A6), but are the unit north and east vectors for the site under consideration.

[67] Source code of the programs for computation of the displacements caused by the atmospheric pressure loading is available on the Web at http://gemini.gsfc.nasa.gov/aplo.

References

Darwin, G. H. (1982), On variations in the vertical due to elasticity of the Earth's surface, *Philos. Mag., Ser. 5*, *14*(90), 409–427.

de Viron, O., H. Goosse, C. Bizouard, and S. Lambert (2002), High frequency non-tidal of the ocean on the Earth's rotation, paper presented at the 27th General Assembly, Eur. Geophys. Soc., Nice, France.

Dong, D., P. Fang, Y. Bock, M. K. Cheng, and S. Miyazaki (2002), Anatomy of apparent seasonal variations from GPS-derived site position time series, *J. Geophys. Res.*, *107*(B4), 2075, doi:10.1029/2001JB000573.

Dziewonski, A. M., and D. L. Anderson (1981), Preliminary Reference Earth Model, *Phys. Earth Planet. Inter.*, *25*, 297–356.

Farrell, W. E. (1972), Deformation of the Earth by surface loads, *Rev. Geophys.*, *10*, 751–797.

Goosse, H., and T. Fichefet (1999), Importance of ice-ocean interactions for the global ocean circulation: A model study, *J. Geophys. Res.*, *104*, 23,337–23,355.

Kalnay, E., et al. (1996), The NCEP/NCAR 40-year reanalysis project, *Bull. Am. Meteorol. Soc.*, *77*, 437–471.

Lefèvre, F., C. Le Provost, and F. H. Lyard (2000), How can we improve a global ocean tide model at a regional scale? A test on the Yellow Sea and the East China Sea, *J. Geophys. Res.*, *105*, 8707–8725.

Lefèvre, F., F. H. Lyard, C. Le Provost, and E. J. O. Schrama (2002), FES99: A global tide finite element solution assimilating tide gauge and altimetric information, *J. Atmos. Oceanic Technol.*, *19*, 1345–1356.

MacMillan, D. S., and J. M. Gipson (1994), Atmospheric pressure loading parameters from very long baseline interferometry observations, *J. Geophys. Res.*, *99*, 18,081–18,087.

Magie, W. F. (1963), *A Source Book in Physics*, Harvard Univ. Press, Cambridge, Mass.

Manabe, S., T. Sato, S. Sakai, and K. Yokoyama (1991), Atmospheric load effect on VLBI observations, in *Chapman Conference on Geodetic VLBI: Monitoring Global Change, Washington, D. C.; April 22–26, 1991, NOAA Tech. Rep. NOS 137 NGS 49*, pp. 111–122, U.S. Dep. of Comm., Silver Spring, Md.

Matsumoto, K., T. Takanezawa, and M. Ooe (2000), Ocean tide models developed by assimilating TOPEX/POSEIDON altimeter data into hydrodynamical model: A global model and a regional model around Japan, *J. Oceanogr.*, *56*, 567–581.

McCarthy, D. D. (1996), IERS conventions 1996, *Tech. Note 21*, Int. Earth Rotation Serv., Paris.

Milly, P. C. D., and A. B. Shmakin (2002a), Global modeling of land water and energy balances. part I: The Land Dynamics (LaD) model, *J. Hydrometeorol.*, *3*, 283–299.

Milly, P. C. D., and A. B. Shmakin (2002b), Global modeling of land water and energy balances. part II: Land-characteristic contributions to spatial variability, *J. Hydrometeorol.*, *3*, 301–310.

Niell, A. E. (1996), Global mapping functions for the atmosphere delay at radio wavelengths, *J. Geophys. Res.*, *101*, 3227–3246.

Nothnagel, A., M. Pilhatsch, and R. Haas (1995), Investigations of thermal height changes of geodetic VLBI radio telescopes, *Proceedings of the 10th Working Meeting on European VLBI for Geodesy and Astrometry*, edited by R. Lanotte and G. Bianco, pp. 121–133, Agenzia Spaziale Ital., Matera, Italy.

Okubo, S., and D. Tsuji (2001), Complex Green's function for diurnal/semidiurnal loading problems, *J. Geod. Soc. Jpn.*, *47*, 225–230.

Pagiatakis, S. D. (1990), The response of a realistic Earth to ocean tide loadings, *Geophys. J. Int.*, *103*, 541–560.

Petrov, L. (2000a), Estimation of EOP from VLBI: Direct approach, in *Proceedings of the IAU Colloquium 180*, edited by K. J. Johnston, pp. 254–258, U.S. Nav. Obs., Washington, D. C.

Petrov, L. (2000b), Instrumental errors of geodetic VLBI, in *Proceedings of the International VLBI Service for Geodesy and Astrometry 2000 General Meeting, Rep. NASA/CP-2000-209893*, edited by N. Vandenberg and K. Baver, pp. 230–235, NASA Cent. for Aerosp. Inf., Greenbelt, Md.

Petrov, L., and C. Ma (2003), Study of harmonic site position variations determined by very long baseline interferometry, *J. Geophys. Res.*, *108*(B4), 2190, doi:10.1029/2002JB001801.

Ponte, R. M., and R. D. Ray (2002), Atmospheric pressure correction in geodesy and oceanography: A strategy for handling air tides, *Geophys. Res. Lett.*, *29*(24), 2153, doi:10.1029/2002GL016340.

Rabbel, W., and H. Schuh (1986), The influence of atmosphere loading on VLBI-experiments, *J. Geophys.*, *59*, 164–170.

Rabbel, W., and J. Zschau (1985), Static deformation and gravity changes at the Earth's surface due to atmosphere loading, *J. Geophys.*, *56*, 81–99.

Ray, R. D. (1999), A global ocean tide model from TOPEX/POSEIDON altimetry: GOT99.2, *Rep. NASA/TM-1999-209478*, 58 pp., NASA, Greenbelt, Md.

Sovers, O. J., J. L. Fanselow, and C. S. Jacobs (1998), Astrometry and geodesy with radio interferometry: Experiments, models, results, *Rev. Mod. Phys.*, *70*(4), 1393–1454.

Takahashi, F., T. Kondo, Y. Takahashi, and Y. Koyama (2000), Very long baseline interferometer, 243 pp., Ohmsha, Tokyo.

Tierney, C., J. Wahr, F. Bryan, and V. Zlotnicki (2000), Short-period oceanic circulation: Implications for satellite altimetry, *Geophys. Res. Lett.*, *27*, 1255–1258.

Trubytsyn, A. P., and A. V. Makalkin (1976), Deformations of the Earth's crust due to atmospheric cyclones, *Izv. Acad. Sci. USSR Phys. Solid Earth, Engl. Transl.*, *12*, 343–344.

vanDam, T. M., and T. A. Herring (1994), Detection of atmospheric pressure loading using very long baseline interferometry measurements, *J. Geophys. Res.*, *99*, 4505–4518.

vanDam, T. M., and J. Wahr (1987), Displacements of the Earth's surface due to atmospheric loading: Effects on gravity and baseline measurements, *J. Geophys. Res.*, *92*, 1281–1286.

vanDam, T. M., G. Blewitt, and M. B. Heflin (1994), Atmospheric pressure loading effects on Global Positioning System coordinate determinations, *J. Geophys. Res.*, *99*, 23,939–23,950.

Vandenberg, N., (Ed.) (1999), International VLBI Service for Geodesy and Astrometry: Annual report, *Rep. NASA/TP-1999-209243*, 308 pp., NASA Cent. for Aerosp. Inf., Greenbelt, Md.

van den Dool, H. M., S. Saha, J. Schermm, and J. Huang (1997), A temporal interpolation method to obtain hourly atmospheric surface pressure tides in Reanalysis 1979–1995, *J. Geophys. Res.*, *102*, 22,013–22,024.

Velicogna, I., J. Wahr, and H. van den Dool (2001), Can surface pressure be used to remove atmospheric contributions from GRACE data with sufficient accuracy to recover hydrologic signals?, *J. Geophys. Res.*, *106*, 16,415–16,434.

Wunsch, C., and D. Stammer (1997), Atmospheric loading and the oceanic "inverted barometer" effect, *Rev. Geophys.*, *35*, 79–107.

———————————

J.-P. Boy, Ecole et Observatoire des Sciences de la Terre, Université Strasbourg, 5 rue René Descartes, F-67084 Strasbourg Cedex, France. (jpboy@eost.u-strasbg.fr)

L. Petrov, NVI, Inc./NASA Goddard Space Flight Center, Greenbelt, MD 20771, USA. (leonid.petrov@lpetrov.net)